


Article

Synthesis of Methyl Mercaptan on Mesoporous Alumina Prepared with Hydroxysafflor Yellow A as Template: The Synergistic Effect of Potassium and Molybdenum

Chuang Peng ^{1,2,†}, Dong Zeng ^{1,†}, Jianjun Li ³, Shuai Peng ¹, Jun Xiong ¹, Weiming Wang ^{1,*} , Yingming Chen ⁴, Hong Liu ⁴, Hao Liu ⁵ and Rui Qin ^{4,*}

¹ Hubei Provincial Engineering Laboratory for Clean Production and High Value Utilization of Bio-Based Textile Materials, Wuhan Textile University, Wuhan 430200, China; pengchuang@hrbeu.edu.cn (C.P.); d201980168@hust.edu.cn (D.Z.); gwzps211@126.com (S.P.); jxiong@wtu.edu.cn (J.X.)

² College of Materials Science and Chemical Engineering, Harbin Engineering University, Harbin 150001, China

³ College of Chemistry and Chemical Engineering, Xiamen University, Xiamen 361005, China; ljj716@163.com

⁴ College of Resource and Environmental Science, South-Central University for Nationalities, Wuhan 430074, China; chen_yingming@126.com (Y.C.); liuhong@mail.scuec.edu.cn (H.L.)

⁵ State Key Laboratory of Coal Combustion, Huazhong University of Science and Technology, Wuhan 430074, China; liuhao@hust.edu.cn

* Correspondence: wangweiming1212@163.com (W.W.); qinrui@mail.scuec.edu.cn (R.Q.)

† These authors contributed equally to this work and should be considered co-first authors.



Citation: Peng, C.; Zeng, D.; Li, J.; Peng, S.; Xiong, J.; Wang, W.; Chen, Y.; Liu, H.; Liu, H.; Qin, R. Synthesis of Methyl Mercaptan on Mesoporous Alumina Prepared with Hydroxysafflor Yellow A as Template: The Synergistic Effect of Potassium and Molybdenum. *Catalysts* **2021**, *11*, 1365. <https://doi.org/10.3390/catal11111365>

Academic Editor: Weijian Diao

Received: 12 October 2021

Accepted: 9 November 2021

Published: 13 November 2021

Publisher's Note: MDPI stays neutral with regard to jurisdictional claims in published maps and institutional affiliations.



Copyright: © 2021 by the authors. Licensee MDPI, Basel, Switzerland. This article is an open access article distributed under the terms and conditions of the Creative Commons Attribution (CC BY) license (<https://creativecommons.org/licenses/by/4.0/>).

Abstract: K-promoted Mo-based catalysts showed great promise for the hydrogenation of CS₂ to methyl mercaptan (CH₃SH). However, the research on the synergistic effect of K and Mo, and the active site of CS₂ hydrogenation to CH₃SH were unexplored widely. To solve this problem, the synergistic effect of K and Mo in the K-promoted Mo-based catalysts for CS₂ hydrogenation to prepare CH₃SH was investigated. The mesoporous alumina was the support and loaded the active components potassium and molybdenum to prepare the catalyst. The results suggested that the active components K and Mo can not only cooperatively regulate the acid-base sites on the catalyst surface, but also stabilize the molybdate species at +5 valence during the reduction process and increase the Mo unsaturated coordination sites. Combined with the results of the catalytic activity evaluation, indicating that the main active site of the catalysts is the weak Lewis acid-base site, and the strong acidic site and strong alkaline site are not conducive to the formation of CH₃SH. Moreover, the possible catalytic mechanism of CS₂ hydrogenation to CH₃SH on the weak Lewis acid-base sites of the catalysts was proposed. The research results of this paper can provide an experimental basis and theoretical guidance for the design of high-performance CH₃SH synthesis catalyst and further mechanism research.

Keywords: methyl mercaptan; CS₂; alumina; synergistic effect; KMo/Al₂O₃

1. Introduction

Methanethiol, also known as methyl mercaptan (CH₃SH), is one of the raw materials for the industrial production of methionine. At present, methyl mercaptan is mainly synthesized by methanol thiolation (CH₃OH-H₂S method) in industry [1–6], which has some disadvantages, such as high reaction temperature (340–400 °C), many byproducts, and serious three wastes. More and more researchers are mainly focused on finding a more economical and environmentally friendly synthesis routes in recent years. Among them, the catalytic synthesis of CH₃SH from sulfur-containing synthesis gas has aroused great interest among researchers [7–14], but the conversion and yield of CH₃SH are relatively low, which does not meet the requirements of large-scale industrialization. CS₂ is relatively surplus and the price is low at present, and the one-step synthesis of CH₃SH by CS₂ hydrogenation has the advantages of low reaction temperature (260–280 °C) and fewer

three wastes. At present, the study of one-step synthesis of CH_3SH from carbon disulfide (CS_2) hydrogenation is rare [15–17]. Therefore, it is necessary to synthesis of CH_3SH by one-step hydrogenation of CS_2 , which not only has positive significance in promoting and enriching the synthesis of CH_3SH but also can realize clean production, which has good economic and social value.

In the field of catalytic synthesis of methanethiol, transition metal sulfides are generally considered to be the main active phase [10,11,14,17–20]. Among them, MoS_2 -based catalysts promoted by alkali metals have potential application prospects because of their unique properties, such as sulfur resistance, not ease to coking and avoiding expensive deep desulfurization in industry, which have been also widely used in water-gas shift [21–24], syngas to higher alcohols [25–30], hydrodesulfurization [31–34] and hydrogenation [35–38]. The research results of active phase MoS_2 in these fields can also provide some reliable basis for the synthesis of CH_3SH . For example, for the synthesis of higher alcohols from syngas, it is generally believed that the synthesis of higher alcohols mainly occurs on the MoS_2 phase promoted by alkali metals, while the pure MoS_2 phase is beneficial to the formation of hydrocarbons. The Johannes A. Lercher research group [16,18] found a similar view in the process of catalytic synthesis of CH_3SH from carbonyl sulfide. It is considered that the catalyst used has two active phases named the pure MoS_2 phase and the potassium-decorated MoS_2 phase. The synthesis of CH_3SH mainly occurs on the potassium-decorated MoS_2 phase, while the pure MoS_2 phase is beneficial to the formation of by-products. Since the 1990s, Yang's group has carried out a detailed study on the catalytic synthesis of CH_3SH from sulfur-containing syngas [8,9,39–42]. Supported molybdate potassium oxide (Mo-O-K) and molybdenum sulfide potassium (Mo-S-K) catalysts supported on silica and modified catalysts containing Ni, Co and Te promoters were developed. The relationship between the preparation method of the catalyst, the optimization of active components, the optimization of reaction conditions, and the catalytic performance was systematically studied, and the mechanism of synthesis of CH_3SH from sulfur-containing syngas over $\text{MoS}_x\text{-K}^+$ catalyst was proposed [8]. It is considered that the by-product methane is easily formed in the MoS_2 active phase, while the CH_3SH is formed in the Mo-S-K active phase.

Herein, to further insight the effect of active components potassium and molybdenum on the selectivity of CH_3SH and how they cooperate in the synthesis of CH_3SH , we chose mesoporous alumina (Al_2O_3) as the support and loaded active components potassium and molybdenum to prepare catalysts to study the one-step synthesis of CH_3SH by CS_2 hydrogenation. The mesoporous alumina was prepared in an aqueous system using hydroxysafflor yellow A derived from safflower as a template. In recent years, our research group has been committed to the research and application development of safflower [43,44]. Due to its unique molecular framework rigidity and reaction with metal ions, hydroxysafflor yellow A in safflower is expected to be used as an ideal template for the preparation of mesoporous alumina in an aqueous system. For $\text{K-Mo/Al}_2\text{O}_3$ catalyst, K and Mo loading and their molar ratio are in the optimal range for CS_2 hydrogenation to CH_3SH . The results of the catalytic activity evaluation showed that the selectivity of by-product CH_3SCH_3 was higher when the catalyst was loaded with a single active component, for example, the selectivity of CH_3SCH_3 was as high as 92.9% at 260 °C on the K/Al catalyst. When K and Mo were introduced simultaneously, the selectivity of CH_3SH increased rapidly, and it reached 91.2% at 260 °C over the K-Mo/Al catalyst. Moreover, the synergistic effect of K and Mo was discussed, and the possible catalytic mechanism for the hydrogenation of CS_2 to CH_3SH on the active site was proposed.

2. Results and Discussion

2.1. Catalytic Performances of the Catalysts

The relationship between the selectivity of the products and the reaction temperature over Al , Mo/Al , K/Al , and K-Mo/Al catalysts is shown in Figure 1. Since the conversion of CS_2 is 100% in the whole reaction temperature range, it is not shown in the figure. It can be seen from Figure 1 that the Al_2O_3 (Al) itself is a highly active catalyst for the hydrogenation

of CS₂. For Al catalyst, the selectivity of CH₃SH, CH₃SCH₃ and CH₄ was 31.5%, 67.5% and 1% at 260 °C, respectively. When the active component Mo is introduced, the changing trend of the selectivity of the products is similar to that of Al catalyst with the increase of reaction temperature, except that the selectivity of CH₃SCH₃ decreases slightly, while the selectivity of CH₃SH increases slightly. As far as K/Al catalyst is concerned, it can be concluded that the addition of potassium alone can greatly reduce the selectivity of CH₃SCH₃, while increasing the selectivity of CH₃SH, that is, the addition of potassium promotes the disproportionation of CH₃SH to CH₃SCH₃, which is especially significant at low temperature (T < 300 °C). When potassium and molybdenum were introduced into the support at the same time, the selectivity of CH₃SH was greatly improved over K-Mo/Al catalyst, and the selectivity of CH₃SH reached 91.2%, the selectivity of CH₄ was only 0.1% at 260 °C; even at 300 °C, the selectivity of CH₃SH was 85.8%, and the selectivity of CH₄ was 1.5%; which shows that the disproportionation and further hydrogenation process of methyl mercaptan are inhibited with the addition of potassium and molybdenum. In addition, for all catalysts, the selectivity of CH₄ increases with the increase of reaction temperature, which is consistent with the reports in the literature [15,16]. For example, the selectivity of CH₄ on K-Mo/Al catalysts is 0.1%, 1.5%, 9.5%, and 25.2% at 260, 300, 340 and 380 °C, respectively, which increased about 16.8 times from 300 to 380 °C (Figure S1). To sum up, we can conclude: when the active component potassium or molybdenum is introduced alone, it is not conducive to the formation of CH₃SH, and when potassium and molybdenum are added at the same time, potassium and molybdenum can play a synergistic catalytic role and jointly promote the formation of CH₃SH.

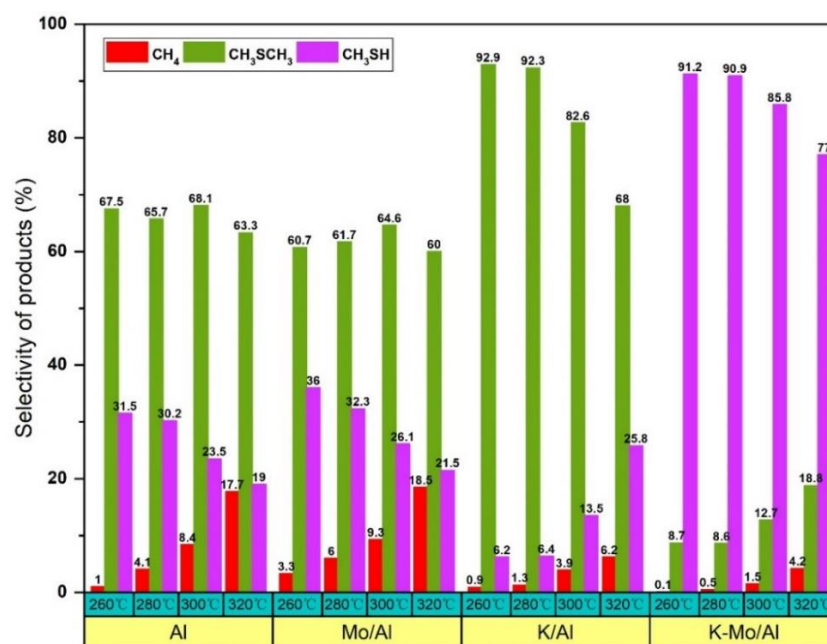


Figure 1. The selectivities toward CH₄, CH₃SCH₃ and CH₃SH as a function of reaction temperature over the Al, Mo/Al, K/Al and K-Mo/Al catalysts. Reaction conditions: $p = 0.3$ MPa, $R(\text{CS}_2) = 1.6$ mL/h, $R(\text{H}_2) = 30$ mL/min, 2 mL of the Catalyst.

2.2. Textural Properties

The fundamental physical and chemical properties of Al, Mo/Al, K/Al and K-Mo/Al catalysts, including BET specific surface area, pore volume and average pore size, are shown in Figure 2. It can be seen from the figure that the specific surface area and pore volume of alumina decrease rapidly with the addition of potassium and molybdenum. For instance, the specific surface area and pore volume of alumina (Al) are 327 m²·g^{−1} and 0.41 cm³·g^{−1} respectively, while that of the K-Mo/Al catalyst are 196 m²·g^{−1} and 0.31 cm³·g^{−1} respectively, which may be largely due to the increase of catalyst density

after the addition of potassium and molybdenum, causing the surface area per unit mass is reduced. At the same time, it was found that the average pore size increased with the addition of potassium and molybdenum, which were 2.55, 2.98, 3.64 and 2.99 nm respectively on Al, Mo/Al, K/Al and K-Mo/Al catalysts, which may be due to the formation of some large particle species with the introduction of potassium and molybdenum during the preparation of the catalyst, resulting in some small pores being blocked.

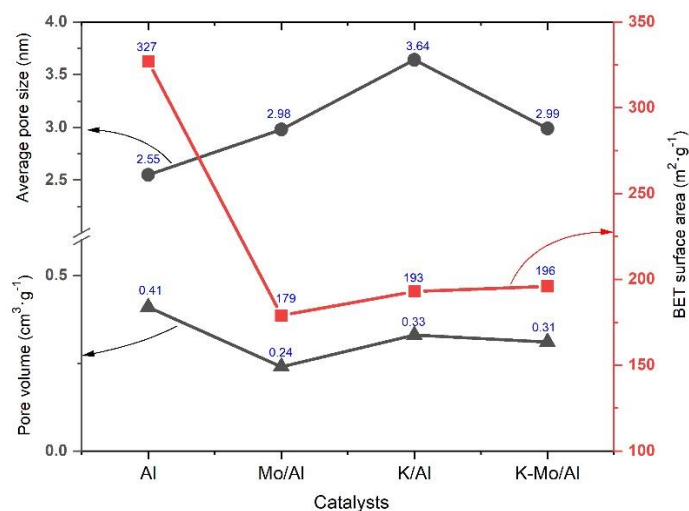


Figure 2. The textural parameters of Al, Mo/Al, K/Al and K-Mo/Al catalysts.

2.3. Crystalline Phase and Morphology

The crystalline phases of Al, Mo/Al, K/Al and K-Mo/Al catalysts before and after reaction were characterized by X-ray diffraction, the XRD patterns are shown in Figure 3. Because the crystalline phase of pure alumina (Al) does not change before and after the reaction, the spectra of the spent Al are not listed in the diagram. The diffraction peak of Al_2O_3 was detected on all the catalysts [JCPDS File Number: 00–029–0063]. The diffraction peaks of $2\theta = 12.5, 23.3, 25.5, 27.3, 33.5, 35.5$ and 56.3° belonging to MoO_3 [JCPDS File Number: 00–005–0508] were detected on the fresh Mo/Al catalyst, while on the spent Mo/Al catalyst, there were mainly diffraction peaks belonging to MoS_2 [JCPDS File Number: 00–024–0513], and the diffraction peak belonging to MoO_2 [JCPDS File Number: 01–078–1070] was detected at $2\theta = 26^\circ$ at the same time. In the case of the K/Al catalyst, the diffraction peaks of $\text{K}_2\text{Al}_{19}\text{O}_{29.5}$ [JCPDS File number: 00044–1009] and K_2O [JCPDS File number: 01–089–5956] were detected on the fresh catalyst, which was consistent with the results of the scanning electron microscope (Figure 4b). The results of SEM showed that new species were formed on the surface of the K/Al catalyst. However, only the diffraction peak belonging to K_2SO_4 [JCPDS File Number: 00–0030608] was detected on the spent catalyst. When potassium and molybdenum were introduced at the same time, no diffraction peaks belonging to potassium and molybdenum species were detected on the fresh K-Mo/Al catalyst, indicating that they were amorphous or highly dispersed on the surface of $\gamma\text{-Al}_2\text{O}_3$, which was consistent with the results of the corresponding EDS mapping images (Figure 4e–h). While on the spent K-Mo/Al catalyst, diffraction peaks belonging to MoS_2 and K_2SO_4 were detected at the same time. According to the report of references [16,18], the active phase MoS_2 phase is formed during the pre-sulfurization process, while the K_2SO_4 phase is formed through the intermediates K_2MoS_4 and K_2S in the activity evaluation process. The sulfided K_2MoS_4 is first transformed into K_2S , and then the irreversible reaction between K_2S and oxygen-containing species leads to the accumulation of the K_2SO_4 phase. Whereas, we did not detect the diffraction peaks of K_2MoS_4 and K_2S species in the XRD diffraction pattern, indicating that K_2MoS_4 and K_2S species are highly dispersed on the alumina support. In addition, we did not perform a pre-sulfurization process for the catalysts before evaluating the activity of the catalysts,

indicating the catalysts can be sulfided by using sulfur-containing raw materials and product H_2S in the reaction process. Finally, on the spent Mo/Al catalyst, not only the diffraction peak of MoS_2 species was detected, but also the diffraction peak belonging to MoO_2 species was detected, demonstrating molybdenum oxide had not been completely sulfided at this time.

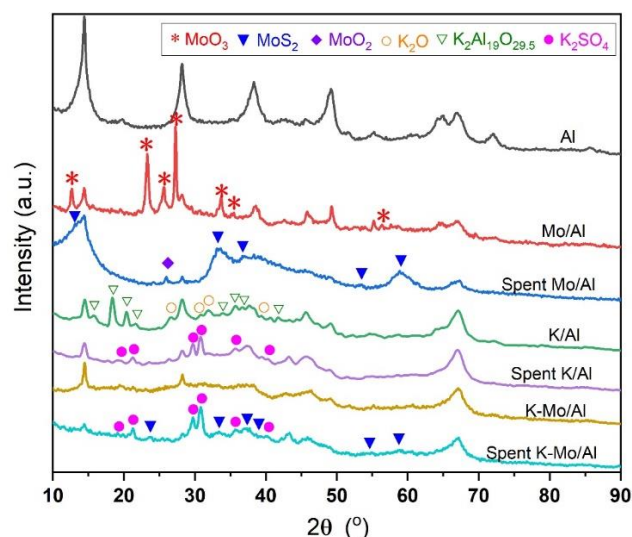


Figure 3. XRD diffraction patterns of the fresh catalysts and the spent catalysts.

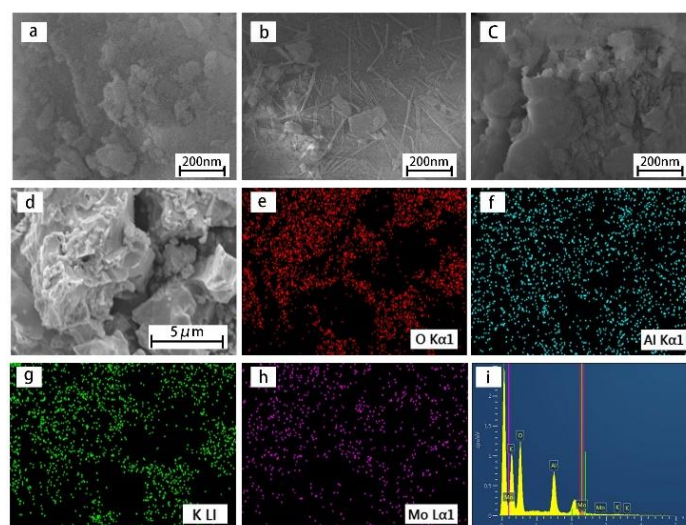


Figure 4. (a) SEM image of the fresh Mo/Al catalyst, (b) SEM image of the fresh K/Al catalyst, (c) SEM image of the fresh K-Mo/Al catalyst, (d) SEM image of the fresh K-Mo/Al catalyst and the corresponding EDS mapping images for O (e), Al (f), K (g) and Mo (h), (i) EDS spectra of the fresh K-Mo/Al catalyst.

2.4. H_2 -TPR Studies

The H_2 -TPR characterization of the fresh catalysts is shown in Figure 5. It can be seen that, in terms of Al_2O_3 , there is a weak low-temperature peak at 202 °C and a wide overlapping peak in the range of 250~600 °C which is mainly attributed to the reduction process of Al species. When the active component is loaded, the low-temperature peak shifts to low temperature, while the wide overlapping peak shifts to a higher temperature, indicating that the interaction between the active component and the Al_2O_3 support becomes stronger after loading the active component and a new H_2 consumption peak appears at 633 °C on the Mo-containing catalysts, which is attributed to the reduction of Mo

species. For the attribution of the reduction peak, it is generally believed that Mo species exist in two states: one is a highly dispersed state (monolayer dispersed structure), and the other is aggregated state (double layer or multilayer structure). Monolayer dispersed Mo-O species are easier to be reduced than double-multilayer dispersed Mo-O species. Brito et al. [45] observed two kinds of reduction peaks on $\text{MoO}_3/\text{Al}_2\text{O}_3$ catalysts named Mo_I (455–500 °C) and Mo_II (780–860 °C). The former belongs to the partial reduction of Mo species with high dispersion, while the latter belongs to the deep reduction of this species and the reduction of Mo species which are more difficult to reduce (such as tetrahedral coordination Mo species). Feng et al. [46] found that the low-temperature reduction peak can be attributed to the reduction process of +6 to +4 valence of octahedral coordination $\text{Mo}(\text{Oh})$ species, and the high-temperature reduction peak is the reduction process of +6 to +4 valence of tetrahedral coordination $\text{Mo}(\text{Td})$ species. It should be pointed out that the distribution of Mo species on the support is often affected by preparation methods, such as the properties of the support, molybdenum precursors, calcination conditions, and other factors. When the temperature is less than 800 °C, the supported molybdenum-oxygen catalyst can't be reduced to the metal state [46,47]. It is generally believed that the molybdenum oxygen species on the support mainly exist in the form of tetrahedral coordination and octahedral coordination, and the molybdenum oxygen species with tetrahedral coordination structures are difficult to be reduced [48]. To sum up, for the Mo/Al and K-Mo/Al catalysts in this paper, the H_2 consumption peak in the range of 250–500 °C can be classified as the Mo (VI)→Mo (IV) reduction process of octahedral molybdenum oxygen species, and at 550–800 °C, it can be attributed to the Mo(VI)→Mo(IV) reduction process of tetrahedral molybdenum species. With the addition of alkali auxiliaries, the surface Mo-O species structure has changed, so that the surface Mo-O structure is more transformed into a tetrahedral structure, and the octahedral coordinated Mo-O species decreases. For the H_2 consumption peak of K-Mo/Al catalyst at low temperature (250–500 °C), the two splitting peaks may be attributed to the Mo (VI)→Mo (V)→Mo (IV) reduction process of octahedral molybdenum species, indicating the addition of alkali can stabilize Mo-O species at +5 valence during the reduction process, which is consistent with the results reported in reference [49,50]. The effect of alkali is considered to delay the reduction of Mo. Chen et al. [51] believe that the addition of alkali strengthens the Mo-O bond and leads to the increase of reduction activation energy.

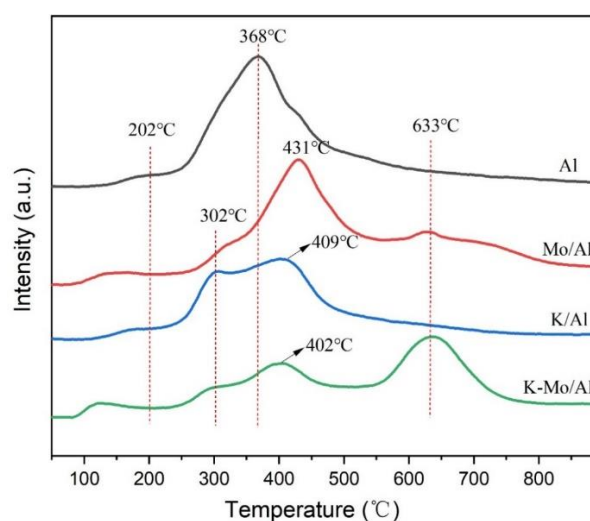


Figure 5. H_2 -TPR spectra of the fresh catalysts.

2.5. Surface Acid-Base Properties

The acid-base sites on the surface of the catalysts are often determined by CO_2/NH_3 -TPD. From the CO_2 -TPD spectrum (Figure 6a), it can be seen that all the catalysts have a CO_2 desorption peak attributed to the weak base center at about 100 °C. There are only

weak basic sites on Al, Mo/Al and K-Mo/Al catalysts, and the quantities of weak base sites decrease greatly when the active component Mo is introduced alone, but when K and Mo are introduced at the same time, the quantities of weak base sites is slightly more than that of the Al catalyst. For the K/Al catalyst, due to the addition of strong basic components, a wide overlapping CO₂ desorption peak belonging to weak, medium and strong basic sites appeared. In addition, according to the NH₃-TPD spectrum (Figure 6b), there are weak, medium and strong acid sites on the surface of the four catalysts, and their relative quantities are summarized in Table 1. Combining the activity evaluation result of the catalyst, it can be considered that strong acid sites and strong base sites are not conducive to the selectivity of methyl mercaptan.

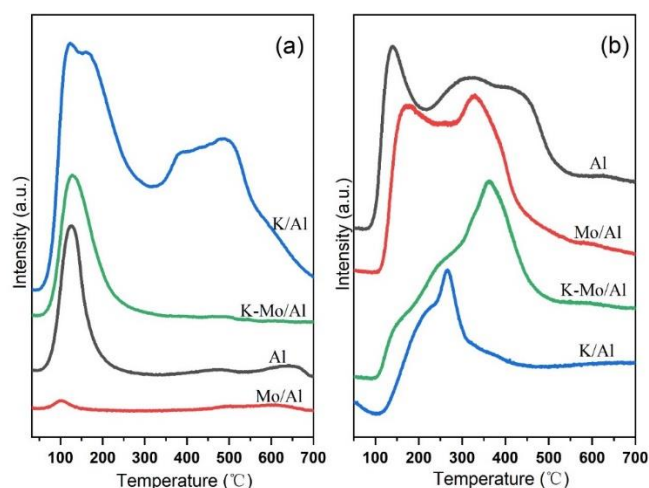


Figure 6. TPD spectra of the catalysts, (a) CO₂-TPD, (b) NH₃-TPD.

Table 1. The quantity distribution of acid-basic sites on the surface of the catalysts.

Catalysts	Basic Site Distribution from CO ₂ -TPD ^[a]				Acid Site Distribution from NH ₃ -TPD ^[a]			
	Weak	Medium	Strong	Total	Weak	Medium	Strong	Total
Al	1.0	-	-	1.0	0.41	0.34	0.25	1.0
Mo/Al	0.03	-	-	0.03	0.53	0.40	0.33	1.26
K/Al	3.67	1.84	2.35	7.86	0.26	0.11	0.03	0.4
K-Mo/Al	1.42	-	-	1.42	0.14	0.15	0.28	0.57

^[a] The quantity of acid sites and basic sites of Al catalyst is defined as 1.0, and other catalysts are compared with it.

The surface acidic sites of the catalysts can also be characterized by pyridine adsorption infrared spectroscopy. As shown in Figure 7, there are five characteristic peaks with different intensities at 1612, 1593, 1577, 1490 and 1444 cm⁻¹, respectively, which are attributed to the different adsorption forms of pyridine on alumina [52]. The absorption peaks at 1612 and 1593 cm⁻¹ belong to the 8a ring vibration mode of the coordination bond between pyridine and Lewis acid site, which belongs to the strong Lewis acid site [4]. When the active component Mo was introduced, a new pyridine desorption peak belonging to the Brønsted acid site appeared at 1540 cm⁻¹, and the intensity of the pyridine desorption peak belonging to the Lewis acid site increased. When K is introduced, all the pyridine adsorption peaks shift to low wavenumber, which may be due to the strong interaction between K and the Al₂O₃ support [4]. The quantities of Lewis acid sites are in the following order: Mo/Al > Al > K/Al > K-Mo/Al. In addition, the intensity of pyridine desorption peak on the surface of K/Al and K-Mo/Al catalysts decreased with the increase of desorption temperature, and pyridine was desorbed completely on K/Al and K-Mo/Al catalysts at 250 °C (Figure S2), indicating that the Lewis acid on the surface of K/Al and K-Mo/Al catalysts is mainly a weak Lewis acid site.

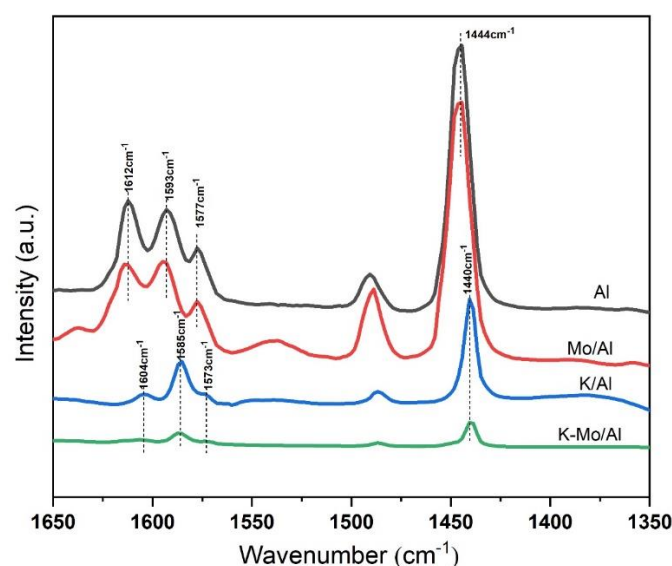


Figure 7. Spectra of pyridine adsorbed on the catalysts at 50 °C.

2.6. XPS Study of Catalysts

The XPS spectra of Mo/Al and K-Mo/Al were shown in Figure 8. The peaks of binding energy at ~229, ~231 and ~232.7 eV represent the +4, +5, and +6 valence states of Mo, respectively, and the acromion at 226.6 eV is the peak of S(2s) [53,54]. Molybdenum species on fresh catalysts are present mainly in the form of Mo⁶⁺, and Mo⁴⁺ appears after the reaction, which is consistent with the results of XRD experiments (Figure 3). MoS₂ (Mo⁴⁺) was detected in XRD experiments on both Mo/Al and K-Mo/Al catalysts after the reaction.

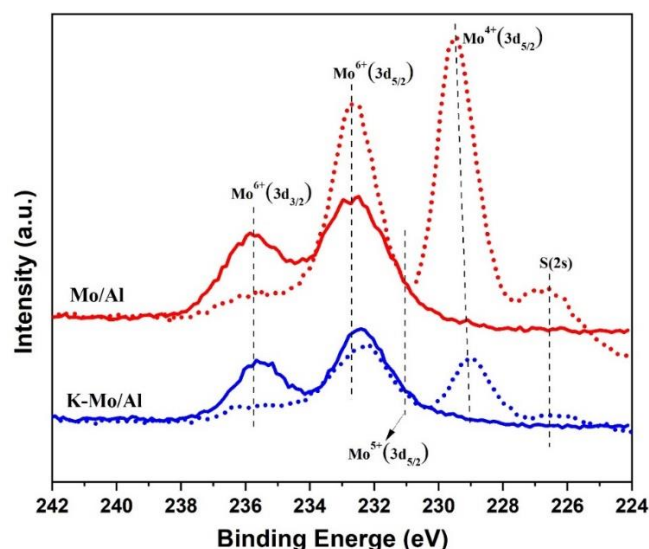


Figure 8. Mo(3d) XPS spectra of the fresh catalysts (Solid line) and the spent catalysts (Dashed line).

The fitting results of the Mo(3d) XPS spectra are shown in Figure 9, and the quantitative results are shown in Table 2. From the results of Table 2, it can be seen that the addition of potassium affects the valence equilibrium among Mo species, increasing the concentration of Mo⁵⁺ species and decreasing the concentration of Mo⁴⁺ species on the sulfided K-Mo/Al catalyst, reducing the reducibility of K-Mo/Al catalyst, which was consistent with the characterization results of H₂-TPR. The research results [46,48,55] show that the Mo-O species mainly have octahedral and tetrahedral configurations, and tetrahedral configurations are more difficult to reduce and sulfurization than octahedral configurations.

Due to the interaction between K and Mo, some octahedral species are transformed into tetrahedral species, so the addition of potassium reduces the reducibility of molybdenum species, resulting in that the Mo^{5+} species being more stable on the K-Mo/Al catalyst, while the Mo^{4+} species is more likely to be formed on the Mo/Al catalyst, which is consistent with the results reported by Kantschewa et al. [55] and Ozkan et al. [50]. Some scholars [51] believe that the addition of alkaline auxiliaries inhibits the reducibility of MoO_3 , and the existence of alkali enhances the bond energy of the Mo-O bond and increases the activation energy of reduction.

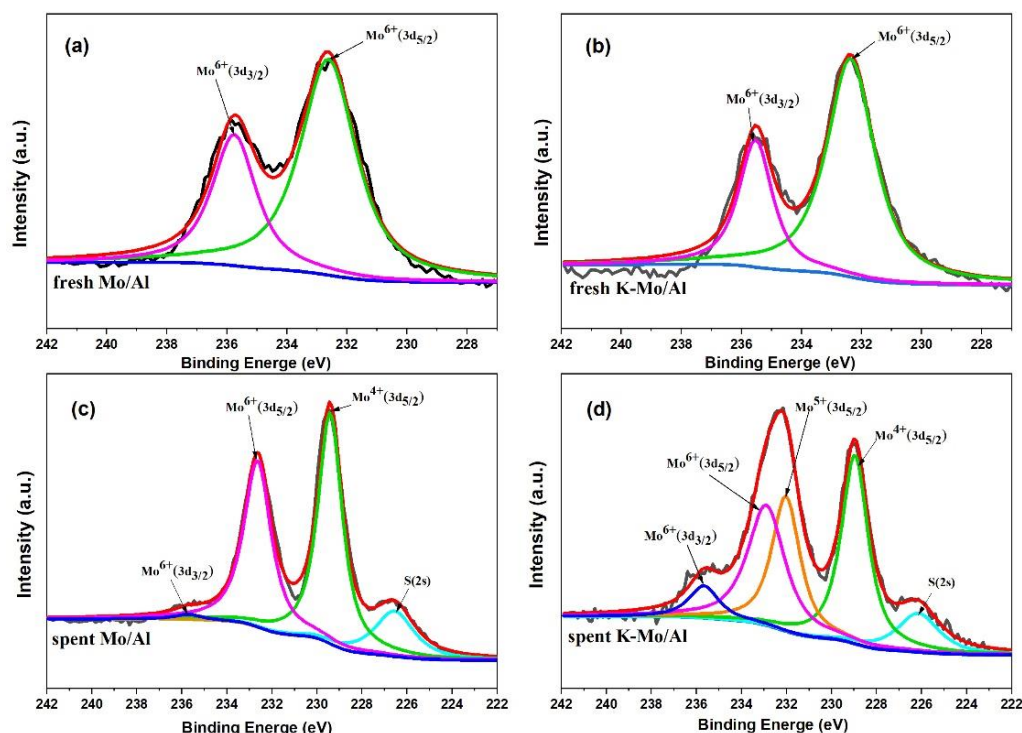


Figure 9. The fitting curves of Mo(3d) XPS spectra of (a) fresh Mo/Al, (b) fresh K-Mo/Al, (c) spent Mo/Al and (d) spent K-Mo/Al.

Table 2. The fitting results of Mo(3d) XPS spectra of the spent catalysts.

Catalysts	Binding Energy of Mo(3d _{5/2}) eV			Concentration (%)		
	Mo ⁴⁺	Mo ⁵⁺	Mo ⁶⁺	Mo ⁴⁺	Mo ⁵⁺	Mo ⁶⁺
Mo/Al	229.4	-	232.6	55.1	0	44.9
K-Mo/Al	229.0	232.0	232.9	38.0	30.8	31.2

Figure 10 shows the S(2p) XPS spectrum of the sulfided catalyst, in which S_H represents the sulfur species of high valence state and S_L represents the sulfur species of low valence state. Low-valent sulfur species can be classified into elements S (164.0 eV), S^{2-} (162.0 eV), S_2^{2-} (162.5 eV), oxy-sulfides (162.3~163.2 eV) and polysulfides (162.9~164.4 eV) [56]. The high valence sulfur species is SO_4^{2-} (169.1 eV), confirmed by the XRD experimental results. The XRD experimental results detected the existence of K_2SO_4 (Figure 3), caused by the oxidation of low-valent sulfur species by oxygen-containing species and other oxidants in the reaction system [16,18]. It can be seen from Figure 10 that the addition of K increases the quantities of the high-valence S^{6+} species, while the low-valence sulfur species decreases (Figure 10). For the MoS_2 -based catalyst, it has been proved that low-valent sulfur ions such as S^{2-} and S_2^{2-} can activate hydrogen [57,58]. In the process of reduction and sulfurization of oxidized Mo (VI) species to Mo^{5+} and Mo^{4+} species in CS_2/H_2 atmosphere, the coordination number of Mo-S and Mo-Mo in the sulfided catalyst is significantly less

than that of the oxidized catalyst, and the surface reconstruction occurs, leading to the increase of Mo unsaturated coordination sites on the catalysts surface [49,59], which is beneficial to the formation of methyl mercaptan.

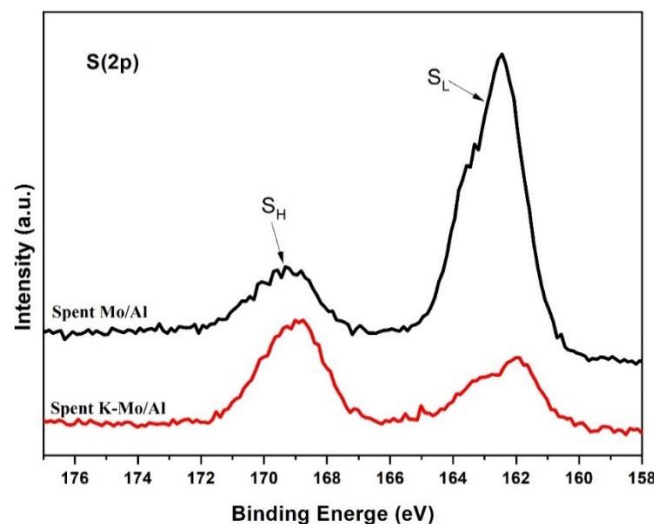


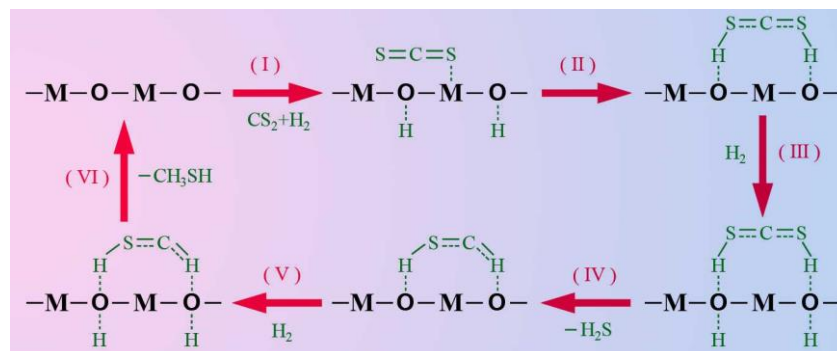
Figure 10. The S(2p) XPS spectra of the spent catalysts.

2.7. Proposed Mechanism on the Acid-Base Site

Combined with the activity test data of the catalysts and the aforementioned characterization results, illustrating the surface performance of the catalysts directly affects the distribution of the products. When alumina is treated with alkali, the Lewis acid site on the surface of the catalyst decreases rapidly, and the strong base site increases greatly, so the selectivity of CH_3SH decreases significantly, and the selectivity of by-product CH_3SCH_3 increases greatly. This is mainly due to the strong adsorption of CH_3SH on the surface of the catalyst, and CH_3SH cannot be separated from the catalyst surface in time, which leads to the further disproportionation of CH_3SH to CH_3SCH_3 . Comparing the activity results of Mo/Al and Al catalysts, the selectivity of CH_3SH on Mo/Al catalyst is slightly higher than that of Al, because the introduction of Mo slightly increases the weak acidity site of the catalyst, which is beneficial to the formation of CH_3SH . After the simultaneous introduction of K and Mo, alkaline K and acidic Mo have a synergistic effect, which jointly regulates the acid-base sites on the surface of the catalyst, thus affecting the adsorption performance of the products on the catalyst surface, and cooperatively catalyzes the hydrogenation of CS_2 to CH_3SH . XPS results show that the increase of Mo^{5+} species concentration on the K-Mo/Al catalyst leads to the increase of Mo coordination unsaturated sites on the catalyst surface, which is beneficial to the activation of CS_2 [15,16,18]. To sum up, as far as the synthesis of CH_3SH by CS_2 hydrogenation is concerned, we have concluded that the main active site of the catalysts is the weak Lewis acid-base site, and the strong acidic site and strong basic site are not conducive to the formation of CH_3SH . In addition, it is generally believed that the active phase for the synthesis of CH_3SH over K-promoted MoS_2 -based catalysts is the K-Mo-S phase [8,10,11,16], but in this paper, we did not pre-sulfurization the catalyst before the reaction, so it can be considered that apart from the K-Mo-S phase, the K-Mo-O phase may also be the main active phase.

The possible reaction mechanism for the hydrogenation of CS_2 to CH_3SH is presented in Scheme 1. Firstly, the molecule H_2 is dissociated and adsorbed on the two adjacent basic centers, while the CS_2 molecule is non-dissociated and adsorbed on the acid site (Step I). The $\text{S}=\text{C}=\text{S}$ double bond is broken and interacts with the nearby dissociated adsorbed H to produce the intermediate fragment HSCSH (Step II). Then, another molecule H_2 is dissociated and adsorbed on the alkaline center (Step III), after the C-S bond breaks and rearranges, the intermediate fragment HSCH is formed, and a molecule of H_2S is

released (Step IV). Finally, another molecule H_2 is dissociated and adsorbed on the base center (Step V), and interacts with the intermediate fragment HSCH and rearranges to form CH_3SH , detached from the surface of the catalyst (step VI). As a result, the catalyst returns to its initial state.



Scheme 1. Reaction mechanism for the hydrogenation of CS_2 to CH_3SH on the weak Lewis acid-base surface centers. (M represents the Lewis acid centers and O represents the Lewis base centers).

3. Experimental Section

For the experimental section, including the preparation, activity tests and characterization of the catalysts, please refer to the Supporting Information for details.

4. Conclusions

In the present study, to further understand the effect of active components potassium and molybdenum on the selectivity of CH_3SH and how they cooperate in the synthesis of CH_3SH , we chose Al_2O_3 as the support and supported active components potassium and molybdenum to prepare catalysts to study the one-step synthesis of CH_3SH by CS_2 hydrogenation. The introduction of alkali metal potassium alone will enhance the surface basicity of the catalyst and lead to the stronger adsorption of the product CH_3SH , which is beneficial to the formation of the by-product CH_3SCH_3 . After loading potassium and molybdenum at the same time, the basic potassium species will interact with the acidic molybdenum species to coordinate the acid-base sites on the surface of the catalyst to promote the formation of CH_3SH . On the K-Mo/Al catalyst, the selectivity of CH_3SH reached 91.2%. The characterization results show that due to the interaction between K and Mo, some octahedral species are transformed into tetrahedral species, so the reducibility of molybdenum species decreases with the addition of K, resulting in the Mo^{5+} species being more stable on the K-Mo/Al catalyst, while the Mo^{4+} species is more likely to be formed on the Mo/Al catalyst. In the process of reduction and sulfurization of oxidized Mo (VI) species to Mo^{5+} and Mo^{4+} species in the reaction atmosphere of CS_2/H_2 , the coordination number of Mo-S and Mo-Mo in the sulfided catalyst decreased significantly compared with that of the oxidized catalyst, and the surface reconstruction occurred, which led to the increase of Mo unsaturated coordination sites on the catalyst surface, which was beneficial to the formation of CH_3SH . In addition, the catalysts were not pre-sulfurization before the reaction, but the presence of MoS_2 was detected in the catalysts after the reaction, indicating that the catalysts can use the reaction atmosphere for self-sulfurization during the reaction. It is considered that apart from the K-Mo-S phase, the K-Mo-O phase may also be the main active phase.

Supplementary Materials: The following are available online at <https://www.mdpi.com/article/10.3390/catal11111365/s1>, Figure S1: The selectivities toward CH_4 , CH_3SCH_3 and CH_3SH as a function of reaction temperature over the Al, Mo/Al, K/Al and K-Mo/Al catalysts. Reaction conditions: $P = 0.3$ MPa, $R(CS_2) = 1.6$ mL/h, $R(H_2) = 30$ mL/min, 2 mL of the Catalyst. Figure S2: Spectra of pyridine adsorbed on the catalysts at (a) 50 °C, (b) 100 °C, (c) 150 °C, (d) 250 °C.

Author Contributions: Conception and design of experiments, W.W. and R.Q.; operation of the experiment, C.P. and D.Z.; data analysis, J.L., S.P. and J.X.; material characterization, Y.C., H.L. (Hong Liu) and H.L. (Hao Liu); writing-original draft preparation, C.P. and D.Z.; writing-review and editing, W.W. and R.Q. All authors have read and agreed to the published version of the manuscript.

Funding: This work was financially supported by the fund of the Key Laboratory of Catalysis and Energy Materials Chemistry of Ministry of Education & Hubei Key Laboratory of Catalysis and Materials Science (CHCL20006), Science and Technology Research Project of Education Department of Hubei Province (Q20181711), the Major Technological Innovation of Hubei Province of China (2018ABA093), the Foundation of State Key Laboratory of Coal Combustion (FSKLCCA2109), and the Foundation of Hubei Provincial Engineering Laboratory for Clean Production and High Value Utilization of Bio-Based Textile Materials (SWJ202109).

Conflicts of Interest: There are no conflict to declare.

References

1. Zhang, Y.H.; Chen, S.P.; Wu, M.; Fang, W.P.; Yang, Y.Q. Promoting effect of SiO_2 on the $\text{K}_2\text{WO}_4/\text{Al}_2\text{O}_3$ Catalysts for Methanethiol Synthesis from Methanol and H_2S . *Catal. Commun.* **2012**, *22*, 48–51. [\[CrossRef\]](#)
2. Bermejo-Deval, R.; Walter, R.M.H.; Gutiérrez, O.Y.; Lercher, J.A. On the Role of the Alkali Cations on Methanol Thiolation. *Catal. Sci. Technol.* **2017**, *7*, 4437–4443. [\[CrossRef\]](#)
3. Pashigreva, A.V.; Kondratieva, E.; Bermejo-Deval, R.; Gutiérrez, O.Y.; Lercher, J.A. Methanol thiolation over Al_2O_3 and WS_2 catalysts modified with cesium. *J. Catal.* **2017**, *345*, 308–318. [\[CrossRef\]](#)
4. Weber-Stockbauer, M.; Gutiérrez, O.Y.; Bermejo-Deval, R.; Lercher, J.A. The Role of Weak Lewis Acid Sites for Methanol Thiolation. *Catal. Sci. Technol.* **2019**, *9*, 509–516. [\[CrossRef\]](#)
5. Weber-Stockbauer, M.; Gutiérrez, O.Y.; Bermejo-Deval, R.; Lercher, J.A. Cesium Induced Changes in the Acid-Base Properties of Metal Oxides and the Consequences for Methanol Thiolation. *ACS Catal.* **2019**, *9*, 9245–9252. [\[CrossRef\]](#)
6. Wang, Y.; Yang, T.L.; Liu, F.; Zhao, T.X.; Wang, X.D.; Cao, J.X. High selectivity in methanethiol synthesis over a coated composite comprising ZSM-5 with t-ZrO₂. *Microporous Mesoporous Mater.* **2020**, *305*, 110358–110365. [\[CrossRef\]](#)
7. Mul, G.; Wachs, I.E.; Hirscho, A.S. Catalytic Synthesis of Methanethiol from Hydrogen Sulfide and Carbon Monoxide over Vanadium-based Catalysts. *Catal. Today* **2003**, *78*, 327–337. [\[CrossRef\]](#)
8. Yang, Y.Q.; Dai, S.J.; Yuan, Y.Z.; Lin, R.C.; Tang, D.L.; Zhang, H.B. The promoting effects of La_2O_3 and CeO_2 on $\text{K}_2\text{MoS}_4/\text{SiO}_2$ catalyst for methanethiol synthesis from synthesis gas blending with H_2S . *Appl. Catal. A* **2000**, *192*, 175–180. [\[CrossRef\]](#)
9. Chen, A.P.; Wang, Q.; Li, Q.L.; Hao, Y.J.; Fang, W.P.; Yang, Y.Q. Direct synthesis of methanethiol from H_2S -rich syngas over sulfided Mo-based catalysts. *J. Mol. Catal. A Chem.* **2008**, *283*, 69–76. [\[CrossRef\]](#)
10. Lu, J.C.; Luo, Y.M.; He, D.D.; Xu, Z.Z.; He, S.F.; Xie, D.L.; Mei, Y. An exploration into potassium (K) containing MoS_2 active phases and its transformation process over MoS_2 based materials for producing methanethiol. *Catal. Today* **2020**, *339*, 93–104. [\[CrossRef\]](#)
11. Yu, M.; Kosinov, N.; Haandel, L.V.; Kooyman, P.J.; Hensen, E.J.M. Investigation of the Active Phase in K-Promoted MoS_2 Catalysts for Methanethiol Synthesis. *ACS Catal.* **2020**, *10*, 1838–1846. [\[CrossRef\]](#)
12. Lu, J.C.; Liu, P.; Xu, Z.Z.; He, S.F.; Luo, Y.M. Investigation of the reaction pathway for synthesizing methyl mercaptan (CH_3SH) from H_2S -containing syngas over K–Mo-type materials. *RSC Adv.* **2018**, *8*, 21340–21353. [\[CrossRef\]](#)
13. Liu, P.; Lu, J.C.; Xu, Z.Z.; Liu, F.; Chen, D.K.; Yu, J.; Liu, J.P.; He, S.F.; Wan, G.P.; Luo, Y.M. The effect of alkali metals on the synthesis of methanethiol from $\text{CO}/\text{H}_2/\text{H}_2\text{S}$ mixtures on the SBA-15 supported Mo-based catalysts. *Mol. Catal.* **2017**, *442*, 39–48. [\[CrossRef\]](#)
14. Cordova, A.; Blanchard, P.; Lancelot, C.; Frémy, G.; Lamonier, C. Probing the Nature of the Active Phase of Molybdenum-Supported Catalysts for the Direct Synthesis of Methylmercaptan from Syngas and H_2S . *ACS Catal.* **2015**, *5*, 2966–2981. [\[CrossRef\]](#)
15. Gutiérrez, O.Y.; Zhong, L.S.; Zhu, Y.Z.; Lercher, J.A. Synthesis of Methanethiol from CS_2 on Ni-, Co-, and K-Doped $\text{MoS}_2/\text{SiO}_2$ Catalysts. *ChemCatChem* **2013**, *5*, 3249–3259. [\[CrossRef\]](#)
16. Gutiérrez, O.Y.; Kaufmann, C.; Lercher, J.A. Synthesis of Methanethiol from Carbonyl Sulfide and Carbon Disulfide on (Co)K-Promoted Sulfide Mo/ SiO_2 Catalysts. *ACS Catal.* **2011**, *1*, 1595–1603. [\[CrossRef\]](#)
17. Wang, W.M.; Zhang, X.; Xia, Z.Q.; Yang, Y.Q. Catalytic synthesis of methanethiol from carbon disulfide and hydrogen over sulfided $\text{KMo}/\text{Al}_2\text{O}_3$ catalysts. *Catal. Lett.* **2015**, *145*, 1521–1528. [\[CrossRef\]](#)
18. Gutiérrez, O.Y.; Kaufmann, C.; Hrabar, A.; Zhu, Y.Z.; Lercher, J.A. Synthesis of methyl mercaptan from carbonyl sulfide over sulfide $\text{K}_2\text{MoO}_4/\text{SiO}_2$. *J. Catal.* **2011**, *280*, 264–273. [\[CrossRef\]](#)
19. Wang, W.M.; Li, Y.; Zhang, X.; Fang, W.P.; Yang, Y.Q. Catalytic synthesis of methanethiol from methanol and carbon disulfide over $\text{KW}/\text{Al}_2\text{O}_3$ catalysts. *Catal. Commun.* **2015**, *69*, 104–108. [\[CrossRef\]](#)
20. Wang, W.M.; Li, J.J.; He, Q.J.; Peng, S.; Li, M. Synthesis of methanethiol from methanol and carbon disulfide over $\text{CoKW}/\text{Al}_2\text{O}_3$ catalysts: The possible reaction network and reaction mechanism. *ChemistrySelect* **2018**, *3*, 9663–9671. [\[CrossRef\]](#)
21. Lund, C.R.F. Microkinetics of Water-Gas Shift over Sulfided Mo/ Al_2O_3 Catalysts. *Ind. Eng. Chem. Res.* **1996**, *35*, 2531–2538. [\[CrossRef\]](#)

22. Liu, B.; Zong, Q.Y.; Edwards, P.P.; Zou, F.; Du, X.; Jiang, Z.; Xiao, T.C.; AlMegren, H. Effect of Titania Addition on the Performance of CoMo/Al₂O₃ Sour Water Gas Shift Catalysts under Lean Steam to Gas Ratio Conditions. *Ind. Eng. Chem. Res.* **2012**, *51*, 11674–11680. [\[CrossRef\]](#)
23. Zhu, T.; Liu, C.; Tan, X.Y.; Huang, B.; Bian, G.Q.; Shao, Q.; Bai, S.X.; Qian, Y.; Li, Y.Y.; Huang, X.Q. Se-Incorporation Stabilizes and Activates Metastable MoS₂ for Efficient and Cost-Effective Water Gas Shift Reaction. *ACS Nano* **2019**, *13*, 11303–11309. [\[CrossRef\]](#) [\[PubMed\]](#)
24. Yun, S.U.; Gulians, V.V. Support Effects on Water Gas Shift Activity and Sulfur Dependence of Mo Sulfide Catalysts. *Energy Fuels* **2019**, *33*, 11655–11662. [\[CrossRef\]](#)
25. Ferrari, D.; Budroni, G.; Bisson, L.; Rane, N.J.; Dickie, B.D.; Kang, J.H.; Rozeveld, S.J. Effect of potassium addition method on MoS₂ performance for the syngas to alcohol reaction. *Appl. Catal. A-Gen.* **2013**, *462–463*, 302–309. [\[CrossRef\]](#)
26. Hensley, J.E.; Pylypenko, S.; Ruddy, D.A. Deactivation and stability of K-CoMoS_x mixed alcohol synthesis catalysts. *J. Catal.* **2014**, *309*, 199–208. [\[CrossRef\]](#)
27. Dorokhov, V.S.; Permyakov, E.A.; Nikulshin, P.A.; Maximov, V.V.; Kogan, V.M. Experimental and computational study of syngas and ethanol conversion mechanisms over K-modified transition metal sulfide catalysts. *J. Catal.* **2016**, *344*, 841–853. [\[CrossRef\]](#)
28. Santos, V.P.; Linden, B.V.D.; Chojecki, A.; Budroni, G.; Corthals, S.; Shibata, H.; Meima, G.R.; Kapteijn, F.; Makkee, M.; Gascon, J. Mechanistic Insight into the Synthesis of Higher Alcohols from Syngas: The Role of K Promotion on MoS₂ Catalysts. *ACS Catal.* **2013**, *3*, 1634–1637. [\[CrossRef\]](#)
29. Zhang, L.F.; Ball, M.R.; Rivera-Dones, K.R.; Wang, S.C.; Kuech, T.F.; Huber, G.W.; Hermans, I.; Dumesic, J.A. Synthesis Gas Conversion over Molybdenum-Based Catalysts Promoted by Transition Metals. *ACS Catal.* **2020**, *10*, 365–374. [\[CrossRef\]](#)
30. Maximov, V.V.; Permyakov, E.A.; Dorokhov, V.S.; Wang, A.J.; Kooyman, P.J.; Kogan, V.M. Effect of Promoter Nature on Synthesis Gas Conversion to Alcohols over (K)MeMoS₂/Al₂O₃ Catalysts. *ChemCatChem* **2020**, *12*, 1443–1452. [\[CrossRef\]](#)
31. Shi, G.J.; Zhao, H.Y.; Song, L.G.; Shen, J.Y. Effect of Solvents on the Hydrogenation and Isomerization of 1-Hexene over Sulfided Co-Mo/γ-Al₂O₃ Catalysts for Hydrodesulfurization. *Energy Fuels* **2008**, *22*, 2450–2454. [\[CrossRef\]](#)
32. Gutiérrez, O.Y.; Singh, S.; Schachtel, E.; Kim, J.; Kondratieva, E.; Hein, J.; Lercher, J.A. Effects of the Support on the Performance and Promotion of (Ni)MoS₂ Catalysts for Simultaneous Hydrodenitrogenation and Hydrodesulfurization. *ACS Catal.* **2014**, *4*, 1487–1499. [\[CrossRef\]](#)
33. Shi, Y.; Wang, G.; Mei, J.L.; Xiao, C.K.; Hu, D.; Wang, A.C.; Song, Y.D.; Ni, Y.; Jiang, G.Y.; Duan, A.J. The Influence of Pore Structure and Acidity on the Hydrodesulfurization of Dibenzothiophene over NiMo-Supported Catalysts. *ACS Omega* **2020**, *5*, 15576–15585. [\[CrossRef\]](#)
34. Mundotiya, S.; Singh, R.; Saha, S.; Kakkar, R.; Pal, S.; Kunzru, D.; Pala, R.G.S.; Sivakumar, S. Effect of Sodium on Ni-Promoted MoS₂ Catalyst for Hydrodesulfurization Reaction: Combined Experimental and Simulation Study. *Energy Fuels* **2021**, *35*, 2368–2378. [\[CrossRef\]](#)
35. Liu, C.; Virginie, M.; Griboval-Constant, A.; Khodakov, A.Y. Potassium promotion effects in carbon nanotube supported molybdenum sulfide catalysts for carbon monoxide hydrogenation. *Catal. Today* **2016**, *261*, 137–145. [\[CrossRef\]](#)
36. Claire, M.T.; Morrill, M.R.; Goh, J.W.; Chai, S.H.; Dai, S.; Agrawal, P.K.; Jones, C.W. Insight into reaction pathways in CO hydrogenation reactions over K/MoS₂ supported catalysts via alcohol/olefin co-feed experiments. *Catal. Sci. Technol.* **2016**, *6*, 1957–1966. [\[CrossRef\]](#)
37. Zeng, F.; Xi, X.Y.; Cao, H.T.; Pei, Y.T.; Heeres, H.J.; Palkovits, R. Synthesis of mixed alcohols with enhanced C³⁺ alcohol production by CO hydrogenation over potassium promoted molybdenum sulfide. *Appl. Catal. B-Environ.* **2019**, *246*, 232–241. [\[CrossRef\]](#)
38. Hu, J.; Yu, L.; Deng, J.; Wang, Y.; Cheng, K.; Ma, C.; Zhang, Q.; Wen, W.; Yu, S.; Pan, Y.; et al. Sulfur vacancy-rich MoS₂ as a catalyst for the hydrogenation of CO₂ to methanol. *Nat. Catal.* **2021**, *4*, 242–250. [\[CrossRef\]](#)
39. Yang, Y.Q.; Yuan, Y.Z.; Dai, S.J.; Wang, B.; Zhang, H.B. The catalytic properties of supported K₂MoS₄/SiO₂ catalyst for methanethiol synthesis from high H₂S-content synthesis gas. *Catal. Lett.* **1998**, *54*, 65–68. [\[CrossRef\]](#)
40. Dai, S.J.; Yang, Y.Q.; Yuan, Y.Z.; Tang, D.L.; Lin, R.C.; Zhang, H.B. On methanethiol synthesis from H₂S-containing synthesis gas over K₂MoS₄/SiO₂ catalysts promoted with transition metal oxides. *Catal. Lett.* **1999**, *61*, 157–160. [\[CrossRef\]](#)
41. Chen, A.P.; Wang, Q.; Hao, Y.J.; Fang, W.P.; Yang, Y.Q. The Promoting Effect of Tellurium on K₂MoO₄/SiO₂ Catalyst for Methanethiol Synthesis from High H₂S-containing Syngas. *Catal. Lett.* **2007**, *118*, 295–299. [\[CrossRef\]](#)
42. Chen, A.P.; Wang, Q.; Hao, Y.J.; Fang, W.P.; Yang, Y.Q. Catalytic Synthesis of Methanethiol from H₂S-rich Syngas Over Sulfided SiO₂-supported Mo-based Catalysts. *Catal. Lett.* **2008**, *121*, 260–265. [\[CrossRef\]](#)
43. Zhang, L.; Zhu, H.; Ke, J.; Qin, R. Selection of a Taxon-Specific Reference Gene for Qualitative and Quantitative PCR Detection of *Carthamus tinctorius*. *Food Anal. Methods* **2017**, *10*, 2952–2963. [\[CrossRef\]](#)
44. Wu, Z.; Liu, H.; Zhan, W.; Yu, Z.; Qin, E.; Liu, S.; Yang, T.; Xiang, N.; Kudrna, D.; Chen, Y.; et al. The chromosome-scale reference genome of safflower (*Carthamus tinctorius*) provides insights into linoleic acid and flavonoid biosynthesis. *Plant Biotechnol. J.* **2021**, *19*, 1725–1742. [\[CrossRef\]](#) [\[PubMed\]](#)
45. Brito, J.L.; Laine, J. Reducibility of Ni-Mo/Al₂O₃ catalysts: A TPR study. *J. Catal.* **1993**, *139*, 540–550. [\[CrossRef\]](#)
46. Feng, L.; Li, X.; Dadyburjor, D.B.; Kugler, E.L. A temperature-programmed-reduction study on alkali-promoted, carbon-supported molybdenum catalysts. *J. Catal.* **2000**, *191*, 1–13. [\[CrossRef\]](#)
47. Arnoldy, P.; de Jonge, J.C.M.; Moulijn, J.A. Temperature-programed reduction of molybdenum(VI) oxide and molybdenum(IV) oxide. *J. Phys. Chem.* **1985**, *89*, 4517–4526. [\[CrossRef\]](#)

48. DeCanio, S.J.; Cataldo, M.C.; DeCanio, E.C.; Storm, D.A. Evidence from XPS for the stabilization of high-valent molybdenum by addition of potassium in Mo/Al₂O₃ catalysts. *J. Catal.* **1989**, *119*, 256–260. [\[CrossRef\]](#)
49. Tatsumi, T.; Muramatsu, A.; Yokota, K.; Tominaga, H. Mechanistic study on the alcohol synthesis over molybdenum catalysts: Addition of probe molecules to CO-H₂. *J. Catal.* **1989**, *115*, 388–398. [\[CrossRef\]](#)
50. Watson, R.B.; Ozkan, U.S. Propane and propylene adsorption effects over MoO_x-based catalysts induced by low levels of alkali doping. *J. Mol. Catal. A* **2003**, *194*, 115–135. [\[CrossRef\]](#)
51. Chen, K.; Xie, S.; Bell, A.T.; Iglesia, E. Alkali Effects on Molybdenum Oxide Catalysts for the Oxidative Dehydrogenation of Propane. *J. Catal.* **2000**, *195*, 244–252. [\[CrossRef\]](#)
52. Rajagopal, S.; Marzari, J.A.; Miranda, R. Silica-alumina-supported Mo oxide catalysts: Genesis and demise of Brønsted-Lewis acidity. *J. Catal.* **1995**, *151*, 192–203. [\[CrossRef\]](#)
53. Baker, M.A.; Gilmore, R.; Lenardi, C.; Gissler, W. XPS investigation of preferential sputtering of S from MoS₂ and determination of MoS_x stoichiometry from Mo and S peak positions. *Appl. Surf. Sci.* **1999**, *150*, 255–262. [\[CrossRef\]](#)
54. Brown, N.M.D.; Cui, N.; McKinley, A. An XPS study of the surface modification of natural MoS₂ following treatment in an RF-oxygen plasma. *Appl. Surf. Sci.* **1998**, *134*, 11–21. [\[CrossRef\]](#)
55. Kantschewa, M.; Delannay, F.; Jeziorowski, H.; Delgado, E.; Eder, S. Nature and properties of a potassium-promoted NiMo/Al₂O₃ water gas shift catalyst. *J. Catal.* **1984**, *87*, 482–496. [\[CrossRef\]](#)
56. Spevack, P.A.; McIntyre, S. Reactivity and stability of sulphided thin films of molybdenum to dry air. *Appl. Catal.* **1990**, *64*, 191–207. [\[CrossRef\]](#)
57. Byskov, L.S.; Bollinger, M.; Nørskov, J.K.; Clausen, B.S.; Topsøe, H. Molecular aspects of the H₂ activation on MoS₂ based catalysts—The role of dynamic surface arrangements. *J. Mol. Catal. A* **2000**, *163*, 117–122. [\[CrossRef\]](#)
58. Startsev, A.N.; Zakharov, I.I.; Parmon, V.N. An unexpected phenomenon in heterogeneous catalysis: Oxidative addition of hydrogen to the sulfide catalysts. *J. Mol. Catal. A* **2003**, *192*, 113–127. [\[CrossRef\]](#)
59. Bian, G.Z.; Fu, Y.L.; Yamada, M. Reaction stability and structure studies of sulfided K-MoO₃/γ-Al₂O₃ catalyst for the synthesis of mixed alcohols. *Appl. Catal. A* **1996**, *144*, 79–91. [\[CrossRef\]](#)